RAA 2016 Vol. **16** No. **12**, 190 (6pp) doi: 10.1088/1674–4527/16/12/190
© 2016 National Astronomical Observatories, CAS and IOP Publishing Ltd.
http://www.raa-journal.org *http://iopscience.iop.org/raa*

***R**esearch in*
***A**stronomy and*
***A**strophysics*

Probing shock geometry via the charge to mass ratio dependence of heavy ion spectra from multiple spacecraft observations of the 2013 November 4 event

Lulu Zhao[1], Gang Li[2,†], Glenn M. Mason[3], Christina Cohen[4], Richard Mewaldt[4], Mihir Desai[5,6], Rob Ebert[5] and Maher Al-Dayeh[5]

[1] Department of Physics and Space Sciences, Florida Institute of Technology, FL 32901, USA
[2] Department of Space Science and CSPAR, University of Alabama in Huntsville, Huntsville, Alabama 35801, USA; *gang.li@uah.edu*
[3] Applied Physics Laboratory, Johns Hopkins University, Laurel, MD 20723, USA
[4] California Institute of Technology, Pasadena, CA 91125, USA
[5] Southwest Research Institute, San Antonio, TX 78228, USA
[6] University of Texas at San Antonio, San Antonio, TX 78249, USA

Received 2016 June 17; accepted 2016 September 6

Abstract In large Solar Energetic Particle (SEP) events, ions can be accelerated at coronal mass ejection (CME)-driven shocks to very high energies. The spectra of heavy ions in many large SEP events show features such as roll-overs or spectral breaks. In some events when the spectra are plotted in terms of energy/nucleon, they can be shifted relative to each other to make the spectral breaks align. The amount of shift is charge to mass ratio (Q/A) dependent and varies from event to event. This can be understood if the spectra of heavy ions are organized by the diffusion coefficients (Cohen et al. 2005). In the work of Li et al. (2009), the Q/A dependence of the scaling is related to shock geometry when the CME-driven shock is close to the Sun. For events where multiple in-situ spacecraft observations exist, one may expect that different spacecraft are connected to different portions of the CME-driven shock that have different shock geometries, therefore yielding different Q/A dependence. In this work, we examine one SEP event which occurred on 2013 November 4. We study the Q/A dependence of the energy scaling for heavy ion spectra using helium, oxygen and iron ions. Observations from *STEREO-A*, *STEREO-B* and *ACE* are examined. We find that the scalings are different for different spacecraft. We suggest that this is because *ACE*, *STEREO-A* and *STEREO-B* are connected to different parts of the shock that have different shock geometries. Our analysis indicates that studying the Q/A scaling of in-situ particle spectra can serve as a powerful tool to remotely examine the shock geometry for large SEP events.

Key words: Sun: particle emission — acceleration of particles

1 INTRODUCTION

Understanding Solar Energetic Particles (SEPs) is a central topic of space plasma research. Studying SEPs provides a unique opportunity to examine the underlying particle acceleration process which exists at a variety of astrophysical sites. Furthermore, understanding SEPs is of practical importance since SEPs are a major concern of space weather. It is now widely accepted that these high energy particles are mostly accelerated at solar flares and shocks driven by coronal mass ejections (CMEs). Events where particles are accelerated mainly at flares are termed "impulsive" (Cane et al. 1986) as the time intensity profile shows a rapid rise and fast decay. In contrast, events where particles are accelerated mainly at CME-driven shocks are termed "gradual" (Cane et al. 1986; Reames 1999) where the time intensity profiles vary gradually compared to impulsive events. For large SEP events, recent studies (e.g. Reames 2009; Cliver 2006; Gopalswamy et al. 2012; Mewaldt et al. 2012) suggested that energetic particles that are observed near Earth in these events are mostly accelerated at the shocks driven by CMEs rather than in flare active regions (ARs).

In many large SEP events, particle fluence spectra exhibit exponential rollover or double power law features (e.g. Mewaldt et al. 2005, 2012). The break energy or the roll-over energy, E_0, is between a few and a few 10s of MeV/nucleon (Mazur et al. 1992; Cohen et al. 2005; Mewaldt et al. 2005; Tylka et al. 2005; Desai et al. 2016b). Simulations (Li et al. 2005) show that spectral breaks can occur naturally for particle acceleration at a CME-driven shock. In examining these features, Cohen et al. (2003, 2005) and Mewaldt et al. (2005) noted that the break en-

ergies are nicely ordered by $(Q/A)^{\sigma}$. They suggested that this ordering can be understood if the energy breaks or roll-overs for different heavy ions occur at the same values of the diffusion coefficient κ. Later, Li et al. (2009) attempted to relate σ to shock geometry. They showed that the value of σ is usually in the range of 1 to 2 for parallel shocks, but can become as small as $\sim 1/5$ for perpendicular shocks.

For the most general case of an oblique shock, the total diffusion coefficient is given by

$$\kappa = \kappa_{||} \cos^2(\theta_{\rm BN}) + \kappa_{\perp} \sin^2(\theta_{\rm BN}). \quad (1)$$

In the above, $\kappa_{||}$ and $\kappa_{\perp}$ are the parallel and perpendicular diffusion coefficients and $\theta_{\rm BN}$ is the angle between the upstream magnetic field and the shock normal. Since in general $\kappa_{||}$ and $\kappa_{\perp}$ have different Q/A dependence (Li et al. 2009), Equation (1) yields a complicated Q/A dependence for the break energy at an oblique shock. Recently, Desai et al. (2016b) have surveyed 0.1–100 MeV/nucleon H-Fe fluence spectra for 46 isolated large gradual SEP events observed at *Advanced Composition Explorer* (*ACE*) during solar cycles 23 and 24. They found that the range of σ for heavy ion spectra in these events is mostly between 0.2 and 2, although some events have a σ value larger than 2.

In the work of Li et al. (2009), it is assumed that the spectral break or roll-over from in-situ observations reflects the same feature of the escaped particle spectra at the shock. We note that some recent calculations have suggested that spectral breaks can emerge as a transport effect (Li & Lee 2015; Zhao et al. 2016). However, in these calculations, the size of the spectral index change is very small, i.e. $\delta\gamma = \gamma_a - \gamma_b$, where γ_a and γ_b are the spectral indices above and below the break energy E_0 respectively. This is in contrast to the observations where $\delta\gamma$ can be large and varies noticeably from one event to another. Furthermore, the transport effect shown in (Li & Lee 2015; Zhao et al. 2016) predicts a Q/A^{σ} dependence of the spectra break energy E_0 with an upper limit of σ being 1.3. In a recent statistical survey, however, Desai et al. (2016a) found that σ in 33 SEP events ranged between $\sim 0.2 - 3$, which clearly exceeds the upper limit of ~ 1.3 predicted by scatter-dominated transport models (Li & Lee 2015; Zhao et al. 2016).

Here we follow Li et al. (2009) and assume that the break is a feature of the escaped particle spectrum at the shock. Note that the Diffusive Shock Acceleration (DSA) does not predict a spectral break for the shock-accelerated particle spectrum. Nevertheless, there could be a variety of reasons for such a break. For example, the break may represent the maximum energy given a finite acceleration time. In this case, we expect the break energies to be high, $>$ several 10s of MeVs for protons. It could also represent the cut-off energy for escape, i.e., particles with energy lower than the break energy are trapped more within the shock complex. In this case, the break energies may be low, $\sim<$ several MeV for protons. In both cases, however, the break energy is decided by the diffusion coefficient κ, so that the same Q/A analysis discussed in the work of Li et al. (2009) applies.

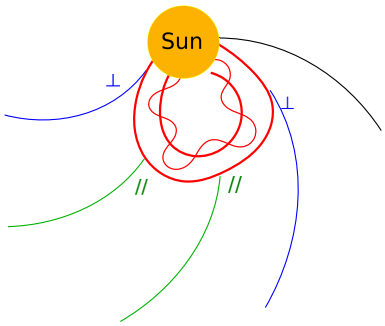

Fig. 1 A diagram showing that two spacecraft can be magnetically connected to different portions of a CME-driven shock which have different shock geometries.

Here we do not discuss the underlying mechanism that leads to the spectral break, but use the Q/A scaling of heavy ion spectra to remotely infer the shock geometry. We note that since particles are continuously accelerated at the CME-driven shock, this shock geometry reflects only an ensemble average of the shock geometry over a period. If, however, the energetic particles near the break energy are mostly accelerated at early times (i.e. in the case of the break energy representing the maximum energy), then we expect that the spectral break reflects the shock geometry when the shock is still close to the Sun.

Since for the same CME the shock geometry differs at different longitudes, then with simultaneous in-situ observations from multiple spacecraft, one may obtain a different Q/A-scaling. This is illustrated in the diagram shown in Figure 1. In the diagram, the two field lines colored in blue (assumed here to be an unperturbed Parker field) intersect with the shock at a quasi-perpendicular configuration and the two field lines colored in green intersect with the shock at a quasi-parallel configuration.

The above discussion indicates that studying the Q/A scaling of heavy ion spectra simultaneously at multiple spacecraft may be used to infer shock geometry of the CME-driven shock for SEP events where heavy ion spectra are well organized by Q/A. In this work, we examine one such SEP event that occurred on 2013 November 4. In the following, we describe the observation in Section 2 and present the fitting results in Section 3. We conclude in Section 4.

2 OBSERVATIONS

We study the SEP event using energetic particle measurements obtained by the Ultra-Low Energy Isotope Spectrometer (ULEIS) (Mason et al. 1998) and Solar Isotope Spectrometer (SIS) (Stone et al. 1998) on *ACE*; and the Suprathermal Ion Telescope (SIT) (Mason et al. 2008) and Low Energy Telescope (LET) (Mewaldt et al. 2008) on the twin spacecraft *Solar TErrestrial RElations Observatory* (*STEREO*) *A* and *B*. On 2013 November 4 00:00 UT, the angle between *ACE* and *STEREO-A* (*STA*) was 148.56°, and the angle between *ACE* and *STEREO-B* (*STB*) was 143.24°. Panel (a) of Figure 2 shows the config-

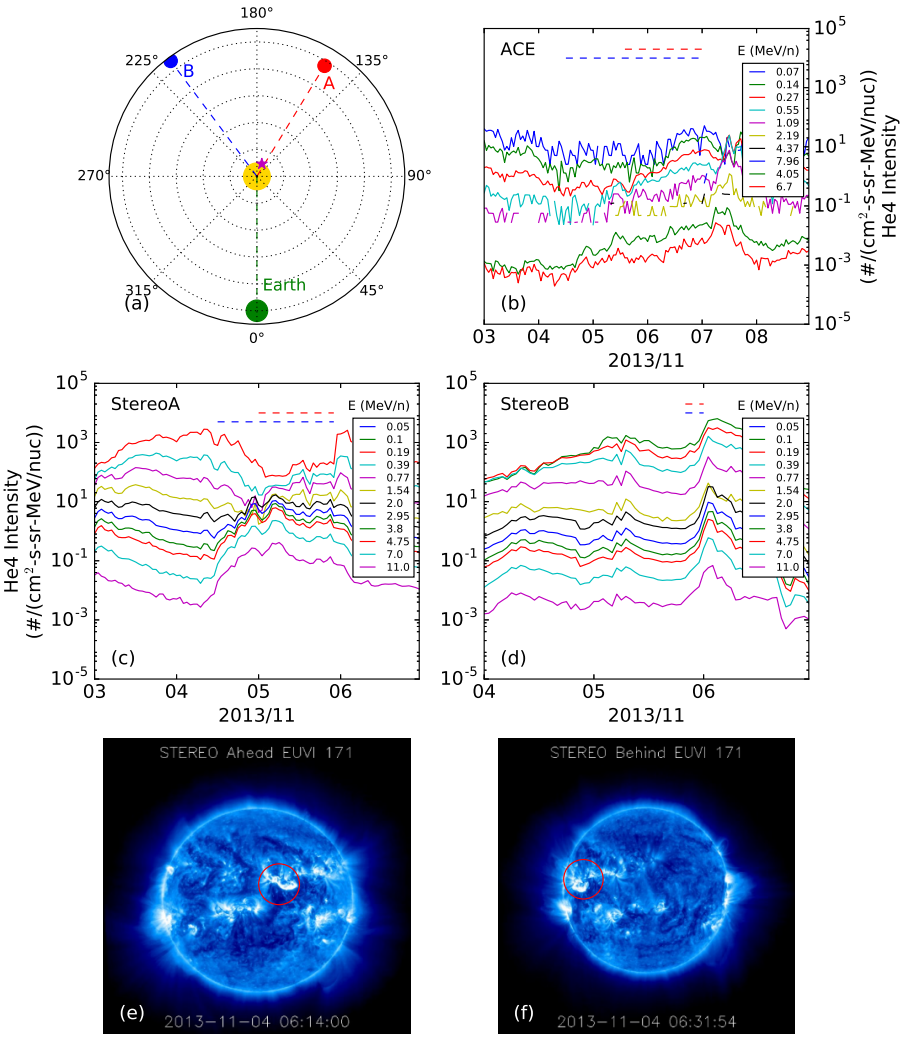

Fig. 2 2013 November 4 SEP event observed by three spacecraft: (a) locations of *STA*, Earth and *STB* at 2013 November 4 00:00 UT, (b) time intensity profiles of ^{4}He observed by *ACE* from 2013 November 3 to November 8, (c) time intensity profiles of ^{4}He observed by *STA* from 2013 November 3 to November 6, (d) time intensity profiles of ^{4}He observed by *STB* from 2013 November 4 to November 6, and (e) and (f) show the EUVI 171 observations of *STA* and *STB* respectively. The AR is marked by the red circle.

uration of *STA*, *STB* and *ACE* for the event and the time intensity profiles of helium for all three spacecraft. The eruption occurred on 2013 November 4 05:12:05 UT as identified from the CME catalog[1]. The event is also included in the survey of Richardson et al. (2014). The event is a backside halo event as viewed from the Earth; a frontside and slightly western event as viewed from *STA*; and an eastern event from *STB*. Without X-ray observations, we do not know the flare class for this event. Panels (e) and (f) show the EUVI 171 observations from *STA* and *STB*. The AR is marked by the red circle.

Panels (b), (c) and (d) of Figure 2 show the time intensity profiles of helium as observed by *ACE*, *STA* and *STB*, respectively. The event was clearly seen at *STA* and *STB*. For *ACE*, even though it was a backside event, one can still see the gradual increase from the background. Note that another event from the same AR had occurred on 2013 November 2 (see Richardson et al. 2014), and the SEPs from that event elevated the intensities at all three spacecraft.

The periods we choose for spectral analysis are shown by the dashed lines in panels (b), (c) and (d). For *STA* and *ACE*, the elevated pre-event background makes it difficult to identify the onset times for the lower energy ions. We therefore use two different periods for different energies: the red dashed lines (November 5 00:00 UT to November 5 22:00 UT) indicate the time interval for the SIT instrument and the blue dashed lines (November 4 12:00 UT to November 5 22:00 UT) indicate the time interval for the LET instrument. Similarly for *ACE* we also use two different periods for different energies: the red dashed lines (November 5 14:00 UT to November 7 02:00 UT) indi-

[1] *http://cdaw.gsfc.nasa.gov/CME_list/UNIVERSAL/2013_11/univ2013_11.html*

cate the time interval for the ULEIS instrument and the blue dashed lines (November 4 12:00 UT to November 7 02:00 UT) indicate the time interval for the SIS instrument. For *STB*, since this is an eastern event, clear increases of the time-intensity profiles do not occur until the end of November 5. So, we choose November 5 20:00 UT to November 6 00:00 UT for all energy channels associated with *STB*. For *STA* and *STB* observations, we choose the stop time of the interval as the time at which the intensities peak. We do not include energetic particles in the downstream. One reason for doing this is that, as shown in Zank et al. (2015), particles can be accelerated at magnetic islands downstream of a shock, leading to an extra acceleration in addition to the shock acceleration. This acceleration may have a different Q/A dependence. Furthermore, turbulence is often stronger downstream of a CME-driven shock and additional second-order Fermi acceleration may occur. Such an acceleration is also Q/A dependent. We, therefore, do not include downstream periods in our analysis. For the *ACE* observation, there was no local shock arrival since it was a backside event. We choose the stop time as November 7 00:00 UT, which is the onset time of a following event.

In obtaining the integrated energy spectra, we only include energy channels that show a clear increase from the background in the time intensity profiles. We do not subtract the pre-event background since the intensities were decaying from a previous event and the identification of a proper pre-event background is difficult. This should not introduce a large uncertainty since the pre-event backgrounds were well below the intensity levels during the chosen time periods.

The pre-event background does affect the time periods we select for obtaining the spectra. As we mentioned above, we use different time periods for *STA*/SIT and *STA*/LET observations. This is because, as shown in panel (c) of Figure 2, the intensities of lower energy helium (below 2 MeV/nucleon) between November 4 12:00 UT and November 5 00:00 UT are still in the decay phase of the previous event. If we assume the intensities in these energy channels behave similarly to that of the ∼2–4 MeV/nucleon channel, then using the 2–4 MeV/nucleon intensity profile as a reference, we can normalize the time integrated intensities for the period denoted by the red dashed line to that denoted by the blue dashed line. In practice, by noting that for helium and oxygen observations there is overlap between the LET energy channel of 4.25 MeV/nucleon and the SIT energy channel of 4.37 MeV/nucleon, we normalize the intensities of all LET energy channels by multiplying a factor (1.8) such that the integrated intensity of the LET 4.25 MeV/nucleon equals that of the SIT energy channel of 4.37 MeV/nucleon. This accounts for the different time intervals used for LET and SIT. We follow the same procedure for calculating the *ACE* spectra and use the energy channel of 4.37 MeV/nucleon of ULEIS and 4.05 MeV/nucleon of SIS for the normalization.

3 RESULTS

We scale Fe and He spectra to match that of O. The scaling can be seen from the following condition

$$\frac{(Q/A)_i^\sigma}{(Q/A)_{\rm O}^\sigma} = \frac{E_i}{E_{\rm O}}\,, \tag{2}$$

where i is He or Fe.

Figure 3 shows the original and scaled time-integrated spectra. Statistical uncertainties are also shown. The upper panels are the original spectra and the lower panels are the spectra after scaling. In the scaled spectra, for better comparison, oxygen spectra are plotted twice, once shifted upward by a factor of 20. The Fe spectra are shifted to the right and the He spectra are shifted to the left to match the "roll-over" features of the O spectra. The spectra of Fe and He are also shifted vertically to make the comparison easier. Statistical uncertainties are shown in the figure. In the following, however, the scaling factors only refer to the energy scaling (i.e. the horizontal shift). For *STA* observations, the energy scaling factor for iron is 2.1; for helium it is 0.80. For *STB* observations, the energy scaling factor for iron is 1.6; for helium it is 0.95. For *ACE* observations, the energy scaling factor for iron is 2.0; for helium it is 0.88.

Assuming the charge state of helium $Q_{\rm He} = 2$, we examine the possible charge state of oxygen in the range of $Q_{\rm O} = 6$ to 7.9. We increase $Q_{\rm O}$ from 6 with a step of $\delta Q = 0.1$. For each $Q_{\rm O}$ we obtain the corresponding σ using Equation (2) with i =He and then using Equation (2) again to obtain the charge state of iron $Q_{\rm Fe}$ with i =Fe. The left panel of Figure 4 shows the value of $Q_{\rm Fe}$ and $Q_{\rm O}$ from our fitting. The red curve is for the *STA* observations, the blue curve is for the *STB* observations and the green curve is for the *ACE* observations. The shaded area in the left panel represents the most probable charge states of oxygen from 6.0 to 7.5 and of iron from 10 to 14 (see discussions below). The right panel shows the corresponding σ value.

For *STA* (red curve), a charge state of oxygen from 6.0 to 7.9 yields a charge state of Fe from 8.1 to 26.5 and the corresponding σ is from 0.8 to 17.7. For *ACE* (green curve), a charge state of oxygen from 6.0 to 7.9 yields a charge state from 4.4 to 25.8 for Fe and a corresponding σ from 0.44 to 10.2. For *STB* (dark blue curve), a charge state of oxygen from 6.0 to 7.9 yields a charge state of 1.5 to 24.6 for Fe and a corresponding σ from 0.18 to 4.1. Note that the range of σ shown in Figure 4 is from 0 to 3, similar to that obtained in Desai et al. (2016b).

The charge states of O and Fe considered by Cohen et al. (2005) are 6.8 and 11.6, respectively. While the charge state for O can be from 6 to 8 for any given SEP event, that for Fe is mostly between 10.0 and 14.0 (e.g. Labrador et al. 2005; Mason et al. 2012). If we vary the charge state of iron $Q_{\rm Fe}$ from 10.0 to 14.0, then from Equation (2) we find a charge state $Q_{\rm O} = 7.23$ to 7.47, and $\sigma = 0.51$ to 0.74 for *STB*; $Q_{\rm O} = 6.88$ to 7.22, and $\sigma = 0.84$ to 1.24 for *ACE*; $Q_{\rm O} = 6.31$ to 6.80, and $\sigma = 0.94$ to 1.78 for *STA*.

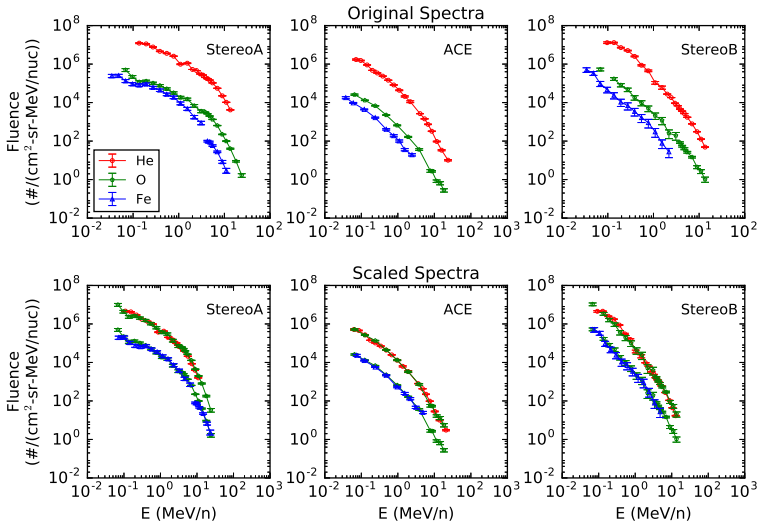

Fig. 3 Spectra of helium, oxygen and iron from *STA*, *ACE* and *STB*, from left to right respectively. *Upper panels* are for the original spectra and *lower panels* are the scaled spectra. Energy spectra are shifted horizontally and vertically to make the comparison easier.

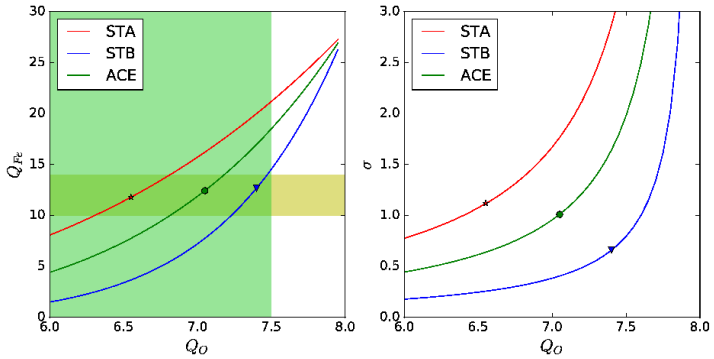

Fig. 4 *Left*: charge state of Fe versus charge state of O. The shaded area represents the most probable charge state of O from 6.0 to 7.5 and of Fe from 10 to 14. *Right*: coefficient σ versus charge state of O.

In Tylka & Lee (2006), the authors argue that the injection energy increases with shock obliquity, leading to a higher Fe/O ratio and higher charge states at quasi-perpendicular shocks. These higher charge states may be from previous impulsive SEP material, which typically has greater energies than solar wind material (Tylka & Lee 2006). Li et al. (2009) obtained a $\sigma \sim 0.22 < 1$ for a perpendicular shock. In our event, the *STB* observation yields a $\sigma < 1$ and may correspond to a quasi-perpendicular portion of the shock. The *STA* observation has a σ larger than 1 for most charge states of iron we considered, and is consistent with a quasi-parallel shock. The *ACE* observations lie in between *STB* and *STA*. If we assume the charge states of both iron and oxygen increase with shock obliquity, and that *STA* (*STB*) is connected to the quasi-parallel (quasi-perpendicular) part of the shock (while *ACE* is connected to a portion of the shock having an obliquity in between *STA*'s and *STB*'s), then a possible choice of ($Q_{\rm Fe}$, $Q_{\rm O}$, σ) can be (12.7, 7.4, 0.66) for *STB*, (12.4, 7.0, 1.01) for *ACE* and (11.8, 6.6, 1.12) for *STA*. We choose these values such that the values of σ increase from *STB* to *ACE* and to *STA*. These choices are labeled as "star," "circle" and "triangle" symbols respectively in Figure 4. This is consistent with the diagram shown in Figure 1 since *STB* saw an eastern event and *STA* saw a central event. For *ACE*, it is a back-side event; the corresponding shock geometry is not clear from Figure 1. Comparing the charge state choices for *STA* and *STB*, we see that for both oxygen and iron, the charge states of the *STB* observation are about 1 unit larger than those of *STA* observations. This difference may reflect the injection and seed population dependence on shock geometry. We remark that direct charge state measurements for energetic particles from future missions such as Interstellar MApping Probe (IMAP) will be helpful in resolving this dependence.

4 DISCUSSION AND CONCLUSIONS

In this paper, we examine the spectra of heavy ions associated with the 2013 November 4 SEP event from *STA*, *STB*

and *ACE*. We select this event because the time-integrated heavy ion spectra from all three spacecraft show spectral break features above ~ 1 MeV/nucleon. Although the pre-event background is elevated due to the presence of SEPs from another event that had occurred two days earlier, time intensity profiles from all three spacecraft show clear increases from the background. Our analyses show that: (1) for all three spacecraft the He, O and Fe spectra can be well organized by Q/A and when scaled by $(Q/A)^{\sigma}$, spectra of different heavy ions overlap nicely; (2) the scaling parameter σ is sensitive to the charge to mass ratio, and for the sets of heavy ion charge states we choose in Section 3, we obtain σ for *STA*, *ACE* and *STB* to be 1.12, 1.01 and 0.66, respectively; (3) Under the framework of Li et al. (2009), these values of σ suggest that *STA* (and *ACE*) are connected to the quasi-parallel part of the shock and *STB* is connected to the quasi-perpendicular part of the shock. This is qualitatively in agreement with the configuration shown by the diagram in Figure 1.

For *ACE* and *STA*, we integrated reasonably long periods (see Fig. 2) to obtain the fluence spectra. As the CME-driven shock propagates out from the Sun to 1 AU, it continues to accelerate particles, but the maximum energy decreases with distance. As a result, the event-integrated spectrum represents an ensemble average of the shock spectra at different times. Since the spectral break feature is around 10 MeV, a reasonably high energy for this event, we expect the dominant contributing particles for *ACE* and *STA* spectra are accelerated close to the Sun, e.g., within 0.3 AU. For *STB*, the period of integration is shorter and close to the shock arrival. Particles of all energies show significant increases from the background at around the same time, indicating that this is due to magnetic connection. This is consistent with the fact that the event is an eastern event as seen from *STB*. For *STB* observations, one may speculate that the spectrum is more local; i.e. the spectrum represents the shock spectrum when the shock is close to 1 AU. However, particles accelerated at earlier times but which are trapped by the CME-driven shock may also contribute. Consequently for the *STB* observation, the range of radial distance of the shock it samples should be larger than those by *ACE* and *STA*. Therefore, when we interpret the result of the Q/A scaling, one needs to be careful in that the shock geometry for the *STB* observation may suffer a larger variation than those from *STA* and *ACE*.

We remark that, as revealed by Figure 4, our analysis may be used not only to obtain shock geometry estimates for multiple spacecraft, but also to examine charge state variability of heavy ions in an event. In principle, one can compare our charge state results with that of ion charge state measurements. However, *ACE*/SEPICA, which measured energetic particle charge states, does not have data after 2005; and both *ACE*/SWICS and *STEREO*/PLASTIC only make charge state measurements at solar wind energies.

Acknowledgements This work is supported at UAH by NSF grants AGS-1135432 and AGS-1622391, NASA grant NNX15AJ93G; at APL by NASA grant NNX13AR20G/115828 (*ACE*/ULEIS and STEREO/SIT) and NASA subcontract SA4889-26309 from the University of California Berkeley; at Caltech by NNX13A66G, NNX11A075G, and subcontract 00008864 of NNX15AG09G and by NSF grant AGS-1156004; at SwRI partially by NSF grant AGS-1460118.

References

Cane, H. V., McGuire, R. E., & von Rosenvinge, T. T. 1986, ApJ, 301, 448
Cliver, E. W. 2006, ApJ, 639, 1206
Cohen, C. M. S., Mewaldt, R. A., Cummings, A. C., et al. 2003, Advances in Space Research, 32, 2649
Cohen, C. M. S., Stone, E. C., Mewaldt, R. A., et al. 2005, Journal of Geophysical Research (Space Physics), 110, A09S16
Desai, M. I., Mason, G. M., Dayeh, M. A., et al. 2016a, arXiv:1605.03922
Desai, M. I., Mason, G. M., Dayeh, M. A., et al. 2016b, ApJ, 816, 68
Gopalswamy, N., Xie, H., Yashiro, S., et al. 2012, Space Sci. Rev., 171, 23
Labrador, A. W., Leske, R. A., Mewaldt, R. A., Stone, E. C., & von Rosenvinge, T. T. 2005, International Cosmic Ray Conference, 1, 99
Li, G., & Lee, M. A. 2015, ApJ, 810, 82
Li, G., Zank, G. P., & Rice, W. K. M. 2005, Journal of Geophysical Research (Space Physics), 110, A06104
Li, G., Zank, G. P., Verkhoglyadova, O., et al. 2009, ApJ, 702, 998
Mason, G. M., Korth, A., Walpole, P. H., et al. 2008, Space Sci. Rev., 136, 257
Mason, G. M., Li, G., Cohen, C. M. S., et al. 2012, ApJ, 761, 104
Mason, G. M., Gold, R. E., Krimigis, S. M., et al. 1998, Space Sci. Rev., 86, 409
Mazur, J. E., Mason, G. M., Klecker, B., & McGuire, R. E. 1992, ApJ, 401, 398
Mewaldt, R. A., Cohen, C. M. S., Labrador, A. W., et al. 2005, Journal of Geophysical Research (Space Physics), 110, A09S18
Mewaldt, R. A., Cohen, C. M. S., Cook, W. R., et al. 2008, Space Sci. Rev., 136, 285
Mewaldt, R. A., Looper, M. D., Cohen, C. M. S., et al. 2012, Space Sci. Rev., 171, 97
Reames, D. V. 1999, Space Sci. Rev., 90, 413
Reames, D. V. 2009, ApJ, 706, 844
Richardson, I. G., von Rosenvinge, T. T., Cane, H. V., et al. 2014, Sol. Phys., 289, 3059
Stone, E. C., Cohen, C. M. S., Cook, W. R., et al. 1998, Space Sci. Rev., 86, 357
Tylka, A. J., Cohen, C. M. S., Dietrich, W. F., et al. 2005, ApJ, 625, 474
Tylka, A. J., & Lee, M. A. 2006, ApJ, 646, 1319
Zank, G. P., Hunana, P., Mostafavi, P., et al. 2015, ApJ, 814, 137
Zhao, L., Zhang, M., & Rassoul, H. K. 2016, ApJ, 821, 62